Paper

Improvement of Performance and Stability of a Drive System with a Low-Resolution Position Sensor by Multirate Sampling Observer

Lilit Kovudhikulrungsri* Member
Takafumi Koseki* Member

This paper describes an effective way to achieve precise information necessary for systems, such as traction drives, where low-resolution position sensors are commonly used. To solve this problem, the authors propose an estimation scheme called multirate sampling observer, which can estimate the state variables during the interval of two consecutive pulses from such sensors. The authors also propose a novel pole placement method that stabilizes the observer in especially in low speed range. The effectiveness of the observer is verified through various simulations and experiments.

Key words: speed estimation, low-resolution sensors, multirate sampling observer, stability

1. Introduction

Low-resolution encoders are normally used as speed sensors in many traction drive systems, such as electric trains, electric vehicles, etc. For example, 60-pulse-per-revolution pulse generators are used to detect speed for electric railway vehicles[(1)] and low-resolution Hall-effect sensors are commonly used in many electric vehicles. Fig. 1 illustrates the sensors. The signals from these kinds of sensors are pulses, which are then used to calculated speed and acceleration. The speed and the acceleration, therefore, are updated only when the next pulse is detected. As a result, the speed and the acceleration cannot be achieved precisely, especially at low speed.

Nowadays, high-frequency digital sampling processors (DSP) are commonly used as controllers. This allows us to precisely control the system. However, it is very difficult to realize in the mentioned systems since the low-resolution sensors are installed. Fig. 2 illustrates the condition at low speed. The period between two consecutive pulses, T_1, is longer than the control period, T_2. It implies that precise control cannot be achieved even though the high-frequency DSPs are used.

To solve this problem, an instantaneous speed observer was proposed to estimate the speed between two consecutive encoder's pulses[(2)]. The instantaneous speed observer is a specific discrete-time observer, which estimates the speed at every sampling time and corrects the estimated speed when the next pulse is detected. As a result, the precise speed is achieved at every sampling time.

* The University of Tokyo
7-3-1 Hongo, Bunkyo-ku, Tokyo, 113-8656

The instantaneous speed observer can also be used to improve the performance of linear scales for linear drives. Its concept is also useful for visual servo, where the sampling rate of the CCD camera is much slower than the sampling rate of the controller. However, the model of the instantaneous speed observer is very specific and limited to motor drive, and its application cannot be extended for the higher order plant such as robot manipulators.

For traction control, one of the difficulties is that it deals with a wide speed range. The authors also applied the instantaneous speed observer for speed estimation of train speed[(3,4,5)]. To apply the instantaneous speed observer, which is designed in discrete-time domain, it is necessary to change the observer gains according to the speed to prevent the noise problem at high speed and instability problem at low speed. The observer gain was tuned by simply considering only the relation of pole locations on *s*- and *z*- planes. As a result, the system can operate stably in a

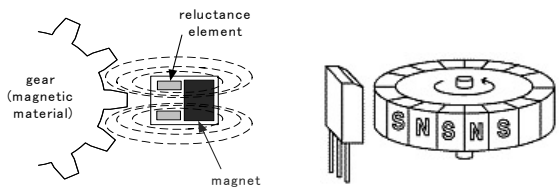

(a) Pulse generator (b) Hall effect sensor

Fig. 1. Examples of low-resolution position sensors

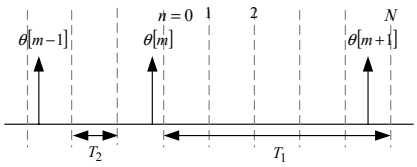

Fig. 2. Encoder pulses at low speed

wide range of speed except at extremely low speed, where pulses cannot be detected frequently. A more systematic gain tuning is necessary to maintain the stability.

In case of the instantaneous speed observer, there are two sampling times, which are the fixed control period T_2 and the variable period between the pulses T_1. Hence, the systematic observer gain tuning can be achieved by using multirate sampling theory[6]. The multirate sampling theory is widely applied in controls of head positioning of hard disk drives[7], virtual servo system of robot manipulators[8], etc. Unlike the other applications of which the ratios of the sampling times are constant, the instantaneous speed observer for traction has variable ratio of the sampling time because of the variable period between the pulses, T_1.

To solve this problem, the authors generalized the instantaneous speed observer based on the multirate sampling theory in order to obtain a systematic gain tuning[9]. The generalized observer has two merits as follows:

- It can be applied to any plants because it is generalized in state space description
- Due to the generalization, the systematic gain tuning is obtained. The stability of the whole system is improved.

The generalized observer will be called multirate sampling observer in this paper. We applied this observer for slip-slide detection in railway traction control and achieved a desirable result compared to the conventional method[10].

In this paper, we will explain the generalization of the multirate sampling observer and the derivation of the systematic tuning of the observer gains in detail. The effectiveness of the observer and the proposed gain tuning method are verified through various simulations and experiments.

2. Multirate Sampling Observer

In this section, the multirate sampling observer, which is generalized from the instantaneous speed observer, and the corresponding gain tuning are described in detail.

2.1 Principle of the instantaneous speed observer

Derivation of the multirate sampling observer is based on the principle of the instantaneous speed observer, which is to estimate the speed between the pulses and correct the error when the next pulse is detected. According to the timing diagram in Fig. 2, the sampling instant $[m,n]$ is defined by

$$t = mT_1(\theta[m]) + nT_2 \equiv [m,n], \quad (1)$$

where $\theta[m]$ denotes the shaft angle. By this definition, it is possible to estimate the rotor speed at any sampling instant $[m,n]$, starting from its value estimated in the previous sampling instant $[m,n\text{-}1]$, if we know the values of the produced torque, T_m, and the disturbance or load torque, T_L. The instantaneous speed observer is described by the following equations:

$$\hat{\omega}[m,n] = \hat{\omega}[m,n-1] + \frac{T_2}{2}\left\{\frac{T_m[m,n] + \hat{T}_L[m] + T_m[m,n-1] + \hat{T}_L[m]}{J}\right\}, \quad (2)$$

where ω is the motor speed in rad/s, J is the moment of inertia and ^ means estimated value.

The error of estimation, which can be corrected when an encoder pulse is detected, is caused by two factors – the deviation of position detection from the encoder, $\Delta\theta$, and the disturbance, ΔT_L. Hence, the update laws have been proposed by

$$\Delta\hat{\omega}[m+1] = \frac{\gamma_1 \Delta\theta[m+1]}{T_1}, \quad (3)$$

$$\Delta T_L[m+1] = \frac{2J\gamma_2 \Delta\theta[m+1]}{T_1^2} \quad (4)$$

The coefficients γ_1 and γ_2 are the weights that allow us to assign the desired estimation error dynamics. It is difficult to obtain the systematic gain tuning from these expressions. Therefore it is necessary to generalize the observer in state space. The generalization will be described in the following section.

2.2 Generalization

Fig.3 shows the block diagram of the multirate sampling observer. RE denotes a low-resolution sensor such as a rotary encoder. The observer is derived from a speed observer in discrete-time domain with consideration of disturbance dynamics.

$$\hat{\mathbf{x}}[n+1] = (\mathbf{A_2} - \mathbf{L_2}\mathbf{C_2})\hat{\mathbf{x}}[n] + \mathbf{B_2}u[n] + \mathbf{C_2}y[n], \quad (5)$$

where $\hat{\mathbf{x}} = \begin{bmatrix}\hat{\theta} & \hat{\omega} & \hat{T}_L\end{bmatrix}^T$, $u = T_m$, $y = \theta$ and $\mathbf{L_2}$ is the observer gain matrix. Note that subscript 2 indicates that the constant control period T_2 is used as the sampling time of the system. Matrices $\mathbf{A_2}$, $\mathbf{B_2}$ and $\mathbf{C_2}$ are derived from their continuous time domain matrices with disturbance consideration $\mathbf{A_{cd3}}$, $\mathbf{B_{cd3}}$ and $\mathbf{C_{cd3}}$, respectively. The subscript 3 means 3rd order. The components of these matrices are described as follows:

$$\mathbf{A_{cd3}} = \begin{bmatrix}0 & 1 & 0\\ 0 & 0 & 1/J\\ 0 & 0 & 0\end{bmatrix}, \mathbf{B_{cd3}} = \begin{bmatrix}0\\ 1/J\\ 0\end{bmatrix}, \mathbf{C_{cd3}} = \begin{bmatrix}1 & 0 & 0\end{bmatrix}. \quad (6)$$

The plant in this case is only the mechanical dynamics of the motor, which can be described as follows:

$$\mathbf{A_c} = \begin{bmatrix}0 & 1\\ 0 & 0\end{bmatrix}, \ \mathbf{B_c} = \begin{bmatrix}0\\ 1/J\end{bmatrix}, \ \mathbf{C_c} = \begin{bmatrix}1 & 0\end{bmatrix}, \mathbf{x} = \begin{bmatrix}\theta\\ \omega\end{bmatrix} \quad (7)$$

Fig. 4 shows a diagram of discrete time signals. Thick and thin arrows denote the detected and estimated signals, respectively. From the diagram, we define an interval between two consecutive

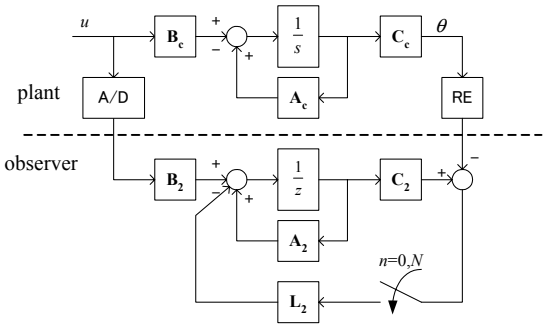

Fig. 3. Block diagram of the multirate sampling observer

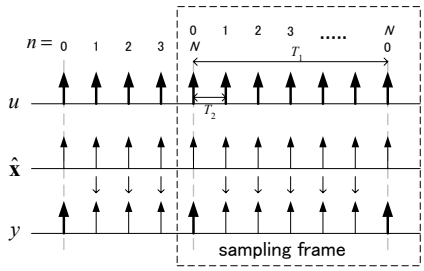

Fig. 4. Discrete time signals

pulses from the encoder as a sampling frame. When an encoder pulse is detected, the error of estimation is corrected. On the other hand, when pulses are not detected, the observer principally works as a simulator, calculating the state variables based on the plant model. This condition is achieved by using the estimated shaft angle when the detected pulses are not available as illustrated in the diagram. This method is practical in both simulations and experiments since it can be programmed easily. This leads to the conclusion that

$$y = \begin{cases} y_{real}, & n = 0, N; N = T_1 / T_2 \\ \hat{y} & \text{otherwise} \end{cases}, \quad \text{..... (8)}$$

where n denotes the sampling index in each sampling frame and N denotes the last sampling instant in each frame. Hence, the observer equations can be expressed as follows:

$$n = 0, ; \hat{\mathbf{x}}[n+1] = \mathbf{A_2}\hat{\mathbf{x}}[n] + \mathbf{B_2}u[n] + \mathbf{L_2}\left(y_{real}[n] - \hat{y}[n]\right), \text{(9)}$$

$$n = 1, \cdots, N-1 ; \quad \hat{\mathbf{x}}[n+1] = \mathbf{A_2}\hat{\mathbf{x}}[n] + \mathbf{B_2}u[n] \text{ . ..... (10)}$$

Due to this fact, the last sampling instant in each sampling frame decides the dynamics of the next sampling frame. Dynamics of each frame can be expressed by

$$\begin{aligned} \hat{\mathbf{x}}[N+1] = {} & \mathbf{A_2}^{n-1}\left(\mathbf{A_2} - \mathbf{L_2}\mathbf{C_2}\right)\hat{\mathbf{x}}[0] + \mathbf{A_2}^{n-1}\mathbf{B_2}u[0] \\ & + \mathbf{A_2}^{n-2}\mathbf{B_2}u[1] + \cdots + \mathbf{A_2}^{0}\mathbf{B_2}u[N-1] \quad \text{.....(11)} \\ & + \mathbf{A_2}^{n-1}\mathbf{L_2}y_{real}[0] \end{aligned}$$

2.3 Pole placement

To place the observer poles, let us rearrange (11) to obtain

$$\hat{\mathbf{X}}[m+1] = \overline{\mathbf{A}}\hat{\mathbf{X}}[m] + \overline{\mathbf{B}}\mathbf{U}[m] + \overline{\mathbf{L}}y[m], \text{ ..... (12)}$$

where $\overline{\mathbf{A}} = \begin{bmatrix} \mathbf{0} & \mathbf{0} & \cdots & \left(\mathbf{A_2} - \mathbf{L_2}\mathbf{C_2}\right) \\ \mathbf{0} & \mathbf{0} & \cdots & \mathbf{A_2}\left(\mathbf{A_2} - \mathbf{L_2}\mathbf{C_2}\right) \\ \vdots & \vdots & \ddots & \vdots \\ \mathbf{0} & \mathbf{0} & \cdots & \mathbf{A_2}^{N-1}\left(\mathbf{A_2} - \mathbf{L_2}\mathbf{C_2}\right) \end{bmatrix}$,

$\overline{\mathbf{B}} = \begin{bmatrix} \mathbf{B_2} & \mathbf{0} & \cdots & \mathbf{0} \\ \mathbf{A_2}\mathbf{B_2} & \mathbf{B} & \cdots & \mathbf{0} \\ \vdots & \vdots & \ddots & \vdots \\ \mathbf{A_2}^{N-1}\mathbf{B_2} & \mathbf{A_2}^{N-2}\mathbf{B_2} & \cdots & \mathbf{B_2} \end{bmatrix}$, $\overline{\mathbf{L}} = \begin{bmatrix} \mathbf{L_2} \\ \mathbf{A_2}\mathbf{L_2} \\ \vdots \\ \mathbf{A_2}^{N-1}\mathbf{L_2} \end{bmatrix}$,

$\hat{\mathbf{X}}[m] = \begin{bmatrix} \hat{\mathbf{x}}[m,1] \\ \hat{\mathbf{x}}[m,2] \\ \vdots \\ \hat{\mathbf{x}}[m.N] \end{bmatrix}$ and $\mathbf{U}[m] = \begin{bmatrix} u[m,0] \\ u[m,1] \\ \vdots \\ u[m, N-1] \end{bmatrix}$.

Poles of the observer are obtained by solving the following equation:

$$\text{eig}(\overline{\mathbf{A}}) = \left|z_2\mathbf{I}_{3N} - \overline{\mathbf{A}}\right| = z_2^{3(N-1)} \cdot \left|z_2\mathbf{I}_3\mathbf{A_2}^{N-1}\left(\mathbf{A_2} - \mathbf{L_2}\mathbf{C_2}\right)\right| = 0, \text{(13)}$$

where z_2 is the z-transform variable due to the constant sampling time T_2, i.e. z_2-domain, which can be obtained by

$$z_2 = \exp(T_2 s) \text{ . .....(14)}$$

The subscript of the identity matrix, $\mathbf{I}$, denotes its dimension. Solving (13), it is found that there are $3N$ poles on z_2-plane in case of the generalized observer in subsection 2.2. Among these, there are only three poles that are not located at the origin. Hence, we can place these three poles by adjusting the observer gain vector $\mathbf{L_2}$, which has three elements.

2.4 Observer gains, pole locations and their relationships when sampled by the variable sampling time T_1 and the constant sampling time T_2

T_1 is defined as the period between two consecutive pulses, so it always varies dependently on motor speed. When dealing with a variable-sampling-time system, the controller and the observer are conventionally designed at a nominal speed or nominal operating point by fixing the poles of z-plane. This method works effectively at nominal speed but the response of the system deteriorates at relatively different speed. The observer equation is described by

$$\hat{\mathbf{x}}[m+1] = \mathbf{A_1}\hat{\mathbf{x}}[m] + \mathbf{B_1}u[m] + \mathbf{L_1}(y[m] - \hat{y}[m]) \text{ .....(15)}$$

Note that subscript 1 indicates that T_1 is used as a sampling time, i.e. z_1-domain. To find the relationship between both domains, let us assume that the input signals in each sampling frame in z_2-domain are constant. At N^{th} sampling instant, based on the fact that

$$\mathbf{A_2}^N = \mathbf{A_1}, \text{.....(16)}$$

and

$$\left(\mathbf{A_2}^{N-1} + \mathbf{A_2}^{N-2} + \cdots + \mathbf{A_2}^{0}\right)\mathbf{B_2} = \mathbf{B_1}, \text{.....(17)}$$

(11) can be rearranged as follows:

$$\hat{\mathbf{x}}[m+1] = \mathbf{A_1}\hat{\mathbf{x}}[m] + \mathbf{B_1}u[m] + \mathbf{A_2}^{N-1}\mathbf{L_2}(y[m] - \hat{y}[m]) \text{ .(18)}$$

Comparing (15) and (18) leads to the following relation

$$\mathbf{L_1} = \mathbf{A_2}^{N-1}\mathbf{L_2} \text{ or } \mathbf{L_2} = \left(\mathbf{A_2}^{N-1}\right)^{-1}\mathbf{L_1} \text{ . .....(19)}$$

Substituting the value of $\mathbf{L_2}$ in (13), neglecting the poles at the origin, and using the fact that $\mathbf{C_1}$ equals to $\mathbf{C_2}$, we obtain

$$\text{eig}(\mathbf{A_1} - \mathbf{L_1}\mathbf{C_1}) = \left|z_1\mathbf{I}_3 - \left(\mathbf{A_1} - \mathbf{L_1}\mathbf{C_1}\right)\right| = 0 \text{ .....(20)}$$

Hence, the poles on z_2-plane that are not located at the origin are identical to the poles on z_1-plane. By this fact, we can calculate the observer gain for the multirate sampling observer in z_1-domain by (20) and convert to z_2-domain by (19). (19) is remarkably important for the stability of the observer. It is necessary to consider the effect of the interval between the pulses.

2.5 Gain tuning procedures

The gain of the multirate sampling observer can be simply tuned by consideration of the relationship of the sampling time T_1 and T_2 or based on (19) and (20) derived in the previous section. The gain tuning procedure is concluded as follows:

1.) Placing the pole on z_1-plane and calculating the observer

gain in z_1-domain, $\mathbf{L_1}$, by using (20)

2.) Using the relationship in (19) to calculate the observer gain in z_2-domain $\mathbf{L_2}$.

The observer gain $\mathbf{L_2}$ is variable according to the number of the intersampling or the ratio of T_1 to T_2, N. In real application, we can easily apply this gain tuning by off-line calculation and using a look-up table.

At low speed, the number of intersampling or the ratio of T_1 to T_2, N, vastly increases. It becomes infinity when the rotating speed drops to zero. This is a substantial difficulty of this observer, since there is still no mathematical proof of the convergence of the observer gains when $N = \infty$. It is necessary to check for the convergence of the gains in advance. If the gains do not converge, the only solution is to determine the operation range and calculate the table. For example, in case of the experiment in section 3, the changes of observer gains converge to some values at large N as shown in Fig. 11. In this case the maximum value of N in this experiment is set to 100. The observer gains are held constant at the values when N=100 if the N exceeds this limit.

3. Simulation and Experimental Verification

The multirate sampling observer and the proposed pole placement are verified by the experimental apparatus shown in Fig. 5. It is composed of an inertia-adjustable drive disk driven by a brushless DC motor and an inertia-adjustable load disk. Both disks are connected to each other by belts via a speed reduction gear set. 16000-ppr rotary encoders are used to measure the speed of each disk but the resolution is reduced to 80 ppr to verify the performance of the observer. List of the parameters and their values are shown in Table 1.

The state equation of the plant is described as follows:

$$\dot{\mathbf{x}} = \mathbf{A}\mathbf{x} + \mathbf{B}u,\ y = \mathbf{C}\mathbf{x} \quad \text{..... (21)}$$

where, $\mathbf{A} = \begin{bmatrix} 0 & 1 & 0 & 0 \\ -\frac{k_{DL}}{g_r^2 J_D} & -\frac{c_D}{J_D} & \frac{k_{DL}}{g_r J_D} & 0 \\ 0 & 0 & 1 & 0 \\ \frac{k_{DL}}{g_r J_l} & 0 & -\frac{k_{DL}}{J_L} & -\frac{c_L}{g_r J_L} \end{bmatrix}$, $\mathbf{B} = \begin{bmatrix} 0 \\ \frac{1}{J_D} \\ 0 \\ 0 \end{bmatrix}$,

$\mathbf{C} = [0 \quad 1 \quad 0 \quad 0]$, $\mathbf{x} = [\theta_D \quad \omega_D \quad \theta_L \quad \omega_L]^T$, $u = T_m$, $y = \omega_D$.

The objectives of the experiments are

- to verify the effectiveness of the proposed pole placement, and
- to confirm the merit of the generalization.

Therefore the experiments are separated into two parts. Table 2 shows the cases of verification. The effectiveness of the proposed pole placement is verified by the simple one-inertia system (case 1 and 2). The order of the multirate sampling observer is three. Then the multirate sampling observer is extended to fifth order in order to apply to the two-inertia system (case 4) and compared with the multirate sampling observer for one-inertia system (case 3) to confirm the merit of the generalization.

3.1 Verification of the proposed pole placement method

The apparatus is set so that the one-inertia system is obtained. The plant is the mechanical dynamics of the motor shown in (7). Therefore, PI controller is used to control the speed of the drive motor in a one-inertia system. Consequently, the third order multirate sampling observer derived in the previous section is enough to estimate the whole state variables. Fig. 6 shows the block diagram of the controlled system.

Pole locations due to conventional pole placement method (calculating the observer gain without consideration of pulse interval, *i.e.* case 1) and the proposed pole placement (calculating the observer gain with consideration of pulse interval, *i.e.* case 2)

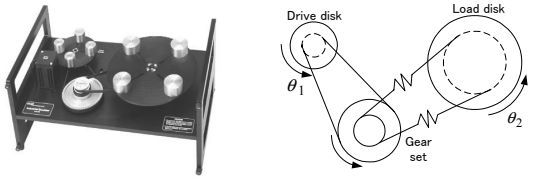

(a) Photograph (b) Free body diagram

Fig. 5. Experimental apparatus

Table 1: List of parameters

Symbol	Description	Value
c_D	Drive friction	0.004 Nm/rad/s
c_l	Load friction	0.05 Nm/rad/s
g_r	Gear ratio	4
J_D	Drive inertia and gear set inertia	0.00252 kgm^2
J_L	Load inertia	0.0271 kgm^2
K_{DL}	Flexible belt's equivalent torsional spring constant	8.45 Nm/rad
θ_D, θ_L	Angle of the drive- and the load disk	
ω_D, ω_L	Speed of the drive- and the load disk	

Table 2: Cases of verification and objectives

Case	Plant inertia	Controller	Observer		Objective
			Order	Gain tuning method	
1	1	PI	3	Conventional	Test of pole placement
2	1	PI	3	Proposed	
3	2	PI	3	Proposed	Test of merit of generalization
4	2	State feedback	5	Proposed	

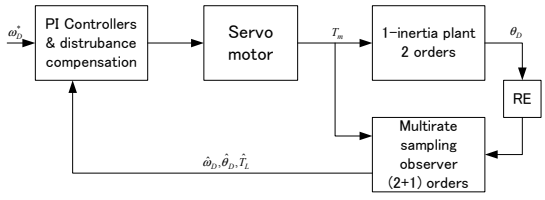

Fig. 6. Block diagram of the controlled system with one-inertia multirate sampling observer

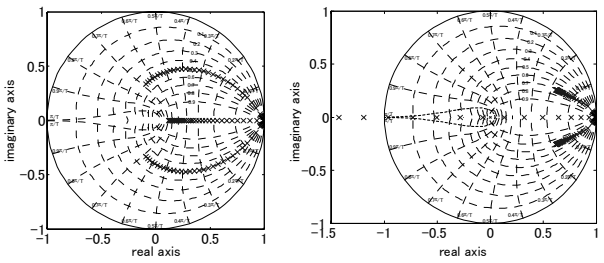

(a) z_1-plane (b) z_2-plane

Fig. 7. Conventional pole placement

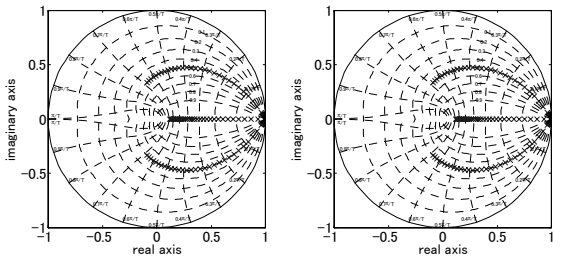

(a) z_1-plane (b) z_2-plane

Fig. 8. Proposed pole placement

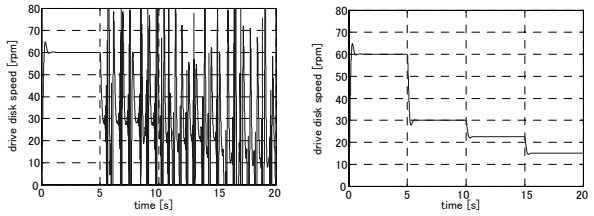

(a) Conventional method (b) Proposed method

Fig. 9. Simulation results comparing the results of the pole placements

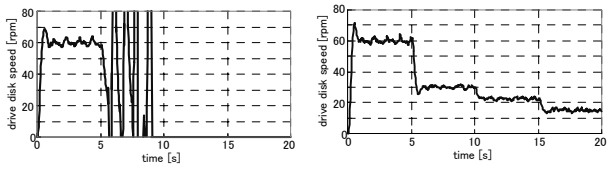

(a) Conventional method (b) Proposed method

Fig. 10. Experimental results comparing of the results of the pole placements

are shown in Fig. 7 and 8, respectively. The poles of the observer are fixed on *s*-plane in order to determine the observer's equivalent time constant. Note that it always twice faster than that of the controlled system. Then, the poles are mapped onto z_1-plane, resulting in the pole movement as shown in Fig. 7(a) and 8(a). The corresponding simulation and experimental results are shown in Fig. 9 and 10, respectively. Note that the size of the look-up table is 100. The observer gains are held constant at the values when N=100 if the N exceeds this limit. In Fig. 7, the poles on z_2-plane that placed by the conventional method move outward the unit circle when speed drops. This finally results in the instability of the system at low speed as shown in Fig. 9(a) and

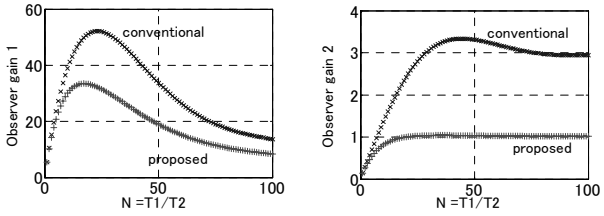

(a) Observer gain 1 (b) Observer gain 2

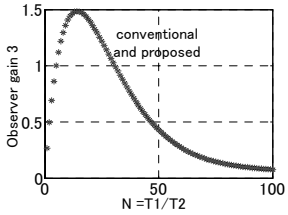

(a) Observer gain 3

Fig. 11. Comparison of the observer gains

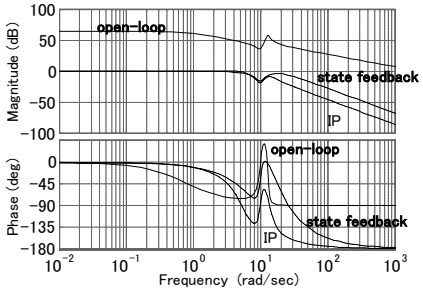

Fig. 12. Frequency response of the two-inertia plant

10(a). On the other hand, Fig. 8 obviously shows that the poles on both planes placed by the proposed method always move inside the unit circle. Therefore, the proposed pole placement maintains the stability of the system at all speed range as shown in Fig. 9(b) and 10(b). Note that the observer time constants are similar in both cases and always faster than that of the controlled system. Comparison of the element of the observer gain vector is shown in Fig. 10. It is obviously seen that the proposed gain tuning method always yields the lower gains.

The system can operate stably until the speed of 15 rpm. The speed of 15 rpm corresponds to the pulse interval (T_1) of 0.05 second in case of the encoder's resolution of 80 ppr and the control period (T_2) is set to 0.001768 second. In other words, T_1 is 28-times greater than T_2. This is very critical in case of the numerical difference method. It is necessary to extend the controlling period; otherwise the error will occur. On the other hand, the multirate sampling observer allows us to design a fast controller even at low speed so the desirable response can be achieved.

3.2 Confirmation of the merit of the generalization

In this section, the merit of the generalization is shown by applying the multirate sampling observer to the two-mass system.

To do this the flexible belt is connected between the load disk and the gear set, separating system into two inertias. The frequency responses of the open- and closed-loop transfer functions are shown in Fig. 12. In case of the original instantaneous speed observer, the observer can estimate only the speed of the motor, so it is not possible to control the whole parameters of the plant. We emulate this condition by using the multirate sampling observer for one-inertia system, which is theoretically equivalent to the original instantaneous speed observer. We call this "the partial multirate sampling observer". It will be compared with the full-state multirate sampling observer, which is extended for two-inertia system.

3.2.1. Partial multirate sampling observer

The experiment is set to case 3 in Table 2. The block diagram of this case and the corresponding experiment results are shown in Fig. 13 and 14, respectively. The reference speed of the drive disk is reduced from 60 to 30, 22.5 and 15 rpm. Since the observer can estimate only the drive disk's parameters so we are able to control only the drive disk. In Fig. 14, the dynamics of the load disk causes the oscillation compared with the case of one-inertia in Fig. 10(b).

3.2.2. Full-state multirate sampling observer

The experiment is set to case 4 in Table 2. In this case the multirate sampling observer is extended so that all state variables are included in the observer model. It can be implemented easily because it is written in state space description. The matrices $\mathbf{A_2}$, $\mathbf{B_2}$ and $\mathbf{C_2}$ in (5) are derived from their continuous time domain matrices with disturbance consideration $\mathbf{A_{cd5}}$, $\mathbf{B_{cd5}}$ and $\mathbf{C_{cd5}}$, respectively. The subscript 5 means 5th order. The components of these matrices are described as follows:

$$\mathbf{A_{cd5}} = \begin{bmatrix} 0 & 1 & 0 & 0 & 0 \\ -\frac{k_{DL}}{g_r^2 J_D} & -\frac{c_D}{J_D} & \frac{k_{DL}}{g_r J_D} & 0 & \frac{1}{J_D} \\ 0 & 0 & 0 & 1 & 0 \\ \frac{k_{DL}}{g_r J_L} & 0 & -\frac{k_{DL}}{J_L} & -\frac{c_L}{J_L} & 0 \\ 0 & 0 & 0 & 0 & 0 \end{bmatrix}, \quad \mathbf{B_{cd5}} = \begin{bmatrix} 0 \\ \frac{1}{J_D} \\ 0 \\ 0 \\ 0 \end{bmatrix}$$

$$\mathbf{C_{cd5}} = \begin{bmatrix} 1 & 0 & 0 & 0 & 0 \end{bmatrix}.$$

The block diagram and the corresponding experimental results are shown in Fig. 15 and 16, respectively. Since the observer can estimate the state variables of both disks, a full state feedback controller can be designed. In Fig. 16, the oscillation is reduced when compared with the case of the PI controller combined with the partial multirate sampling observer in Fig. 14. This fact confirms the merit of the generalization that allows us to design a full-state observer in order to implement the state feedback.

4. Conclusions

This paper has described an effective way to achieve precise information from a low-resolution position sensor by using the multirate sampling observer. This observer can be extended for estimating a high-order plant easily since it has been generalized. This extension has allowed us to estimate the whole state variables. This made the design of state feedback possible and control performance was improved, compared to the conventional methods. To realize the operation of the multirate sampling observer in all speed range, we have proposed a novel pole placement method by considering the relationship between the error correcting and the estimating periods (T_1 and T_2). The effectiveness of the multirate sampling observer has been verified through various simulations and experiments. The results have confirmed that the multirate sampling observer operates stably especially at low speed and can be applied to various plants.

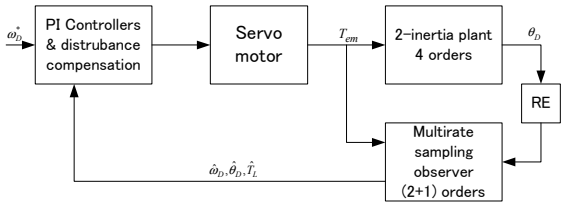

Fig. 13. Block diagram for controlling the two-inertia plant with the partial multirate sampling observer

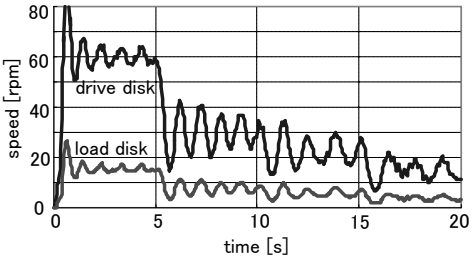

Fig. 14. Experimental result in case of the two-inertia plant and the partial multirate sampling observer

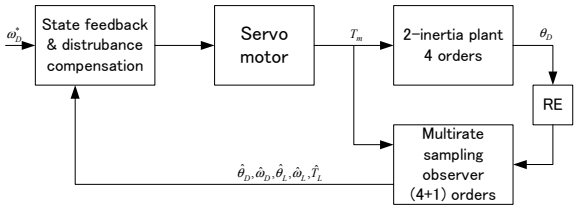

Fig. 15. Block diagram for controlling the two-inertia plant with the full-order multirate sampling observer

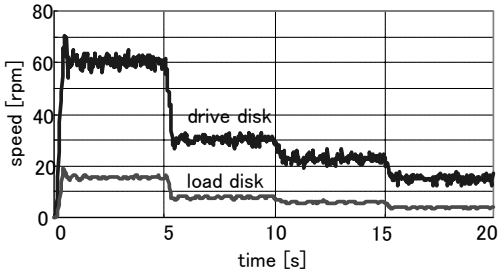

Fig. 16. Experimental result in case of the two-inertia plant and the full-order multirate sampling observer

References

(1) T. Watanabe, "Technical Development Trend of All Electric Brakes" *Rolling Stock & Technology*, no.74, pp. 2-8, 2000.

(2) Y. Hori, "Robust Motion Control Based on a Two-Degrees of-Freedom Servosystem", *Advanced Robotics*, vol.7, No.6, pp.525-546, 1993.

(3) L. Kovudhikulrungsri, T. Koseki: "Stability Analysis of an Instantaneous Speed Observer for an Induction Motor with a Low-Resolution Encoder", *J-RAIL 2000*, pp.349-352, Kawasaki, Dec., 2000.

(4) L. Kovudhikulrungsri, T. Koseki: "Control of an Induction Motor for Pure Electric Brakes", *Proc. 2001 Japan Industry Applications Society Conference*, Vol.3, pp.1297-1303, Matsue, Aug., 2001.

(5) L. Kovudhikulrungsri, T. Koseki, "Precise Speed and Torque control for AC Traction Pure Electric Braking System in Low Speed Range", *Trans. IEE of Japan*, vol. 122-D, no. 11, pp.1027-1033, 2000.

(6) M. Araki, K. Yamamoto, "Multivariable Multirate Sampled-Data System: State-Space Description, Transfer Characteristics and Nyquist Criterion", *IEEE Trans. Automatic Control*, vol. AC-31, pp.145-154, 1986.

(7) H. Fujimoto, Y. Hori, T. Yamaguchi, S. Nakagawa, "Seeking Control of Hard Disk Drive by Perfect Tracking Using Multirate Sampling Control", *Trans. IEE of Japan*, vol. 120-D, no. 10, pp.1157-1164, 2000 (in Japanese).

(8) M. Nemani, T. C. Tsao, S. Hutchinson, "Multi-rate Analysis and Design of Visual Feedback Digital Servo-control System" *ASME J. Dynam. Syst., Measur., and Contr*., vol. 116, pp 44-55, March 1994.

(9) L. Kovudhikulrungsri, T. Koseki, "Control of a Traction Motor at Low Speed with Consideration of Vehicle Dynamics", *Proc. Joint Techinical Meeting on Transportation and Electric Railways and Linear Drives*, pp.35-40, July 2002

(10) L. Kovudhikulrungsri, D. Tateishi, T. Koseki, "Parameter Estimation by Multirate Sampling Observer for Slip-slide Detection", *2003 IEEJ National Convention Record*, Vol.5, pp.304-305, Sendai, Japan, Mar, 2003 (in Japanese)

Lilit Kovudhikulrungsri (Member) was born in Bangkok, Thailand in 1977. He received a Ph.D. degree in electrical engineering from the University of Tokyo in 2004 and joined NSK steering systems co., ltd. His research fields are control systems and electric drives.

Takafumi Koseki (Member) was born in Tokyo in 1963. He received a Ph.D. degree in electrical engineering from the University of Tokyo in 1992 and is presently an associate professor at the Department of Information and Communication, the University of Tokyo. He is studying applications of electrical engineering to public transport system, especially, to linear drives, and analysis and control of traction systems.